Broadband Photosensitive Medium Based on Amorphous Equichalcogenides

Roman Golovchak[a]*, Jarres Plummer[a], Andriy Kovalskiy[a], Yuriy Holovchak[a], Tetyana Ignatova[b], Kyle Nowlin[b], Anthony Trofe[b], Yaroslav Shpotyuk[c,d], Catherine Boussard-Pledel[e], Bruno Bureau[e]

[a]Department of Physics, Engineering and Astronomy, Austin Peay State University, Clarksville, TN 37044, USA

[b]Department of Nanoscience, University of North Carolina, Greensboro, NC 27401, USA

[c]Institute of Physics, University of Rzeszow, Rzeszów, PL-35-959, Poland

[d]Department of Sensor and Semiconductor Electronics, Ivan Franko National, University of Lviv, 107 Tarnavskoho Str., UA-790017 Lviv, Ukraine

[e]University of Rennes 1, CNRS, ISCR [(Institut des Sciences Chimiques de Rennes)] – UMR 6226, F 35000 Rennes, France

*E-mail: holovchakr@apsu.edu

KEYWORDS: chalcogenide glass, photocurrent, light sensitivity, wavelength dependence, temperature dependence.

ABSTRACT: A photosensitive medium based on amorphous equichalcogenide thin films containing germanium and antimony is proposed with characteristics promising for applications in all-chalcogenide photonics, sensorics and photovoltaics. Optical properties, temperature and exposure wavelength dependence of DC electrical conductivity are shown to be comparable with those for halide perovskites, which potentially makes amorphous equichalcogenides a very attractive alternative. The change in dark resistivity with temperature is found to follow exponential decay, covering 2 orders of magnitude over a 70 K temperature interval. Light exposure leads to several orders of relative changes in a current when compared to its dark value. Strong photocurrent response is observed under low power (mW range) exposure across the entire 400-1000 nm range of the investigated wavelengths. An increase in temperature leads to a decrease in the photo-response of the developed material, which is found to vanish at temperatures higher than 120 ^{o}C when only few mW exposure power is used.

1. INTRODUCTION

Amorphous semiconductors are now considered the most promising, cost and energy effective functional materials to replace the crystalline counterparts in many photonic and electronic applications. Besides typical semiconductor properties, these materials also possess a number of features that are unique to the disordered solids, such as glass transition, relative (compare to crystals) insensitivity to small concentration of impurities and defects, externally activated transitions between different metastable states, possibility of crystalline inclusions leading to unique properties at the interfaces, and stimulated crystallization/amorphization phase-change transitions.[1-4] This opens a broad opportunity for engineering of the multifunctional universal

media capable of multitasking, which could potentially improve scalability of devices, simplify technological processes and lead to better integrability within electronic/photonic systems. Chalcogenide glasses and amorphous films are often referred to as canonical materials in the field of amorphous semiconductors and many binary and ternary chalcogenide systems are, therefore, thoroughly studied.[1-8] As a result, a number of compositions are proposed for modern industrial applications, which include data storage devices,[9,10] elements of infrared optics,[11,12] media for reconfigurable meta-optics and optical switches,[13-17] tunable emitters and absorbers,[18,19] nonvolatile photonics,[20-24] solid state electrolytes,[25,26] biosensors[27-29] and many others. By analyzing all these data, it can be noticed that the probability to observe an interesting physical phenomenon or new unique functionality increases dramatically as the number of constituent chemical elements in the composition increases. This is one of the reasons why the focus of current research in the field of chalcogenide material science is gradually shifting towards the multinary (more than 3 chemical elements) chalcogenide-based compositions.[30-32] One of the functionalities, having a significant practical importance, is the possibility to create photosensitive medium capable of detecting light from the broad range of the spectrum through conductivity changes, which can be then integrated into photonics/electronics circuits, photovoltaic or sensor systems. According to modern trends the medium is also required to be scalable, compatible with the flexible electronics concept, integrable with semiconductor technology and obtained by relatively inexpensive synthesis procedures. Amorphous chalcogenides satisfy all these requirements and, compared to the ordinary crystalline or ceramic semiconductors that can be photoexcited by super or bandgap illuminations only, produce a measurable effect under a sub-bandgap light illumination too. Thus, it is known that sub-bandgap photoexcitation can trigger atomic motions in chalcogenide glasses via indirect mechanisms, leading to a dramatic macroscopic effect.[3,33] In

addition, the photo-induced changes produced by super-bandgap light in surface layers (due to a limited penetration depth) can be significantly enhanced unlike that of their crystalline or ceramic counterparts, owing to a strong electron-phonon coupling intrinsic to chalcogenide materials.[33,34] These unique properties lead to an extended sensitivity range of working wavelengths in chalcogenides, which, in combination with a possibility for gradual tuning of physical and chemical properties through composition variation allowed by their amorphous/vitreous nature, pave a way to obtain a quite appealing universal matrix for future integrated electronic-photonic devices.

Experimental studies and theoretical calculations on the valence band structure of chalcogenide glasses[35-37] indicate that the highest occupied molecular orbitals in these materials are usually formed by loosely bonded lone pair electrons of chalcogen atoms (S, Se, Te). These electrons play a key role in the photo and radiation sensitivity of chalcogenides,[3,8,37,38] although the exact mechanisms are not yet fully understood. So far, wavelengths dependence of photocurrent response is studied only in binary/ternary compounds containing one sort of chalcogen atoms (like As_2S_3, As_2Se_3, As_2Te_3,[39-41] Bi-modified As_2Se_3 or Ge-S,[42,43] Sb_2S_3,[3] amorphous Se,[3] Ge-Te thin films,[44] $Ge_2Sb_2Te_5$ and $Ag_4In_3Sb_{67}Te_{26}$ phase-change materials[45] and selected germanium selenides[33]). It was observed that replacing S with Se and then with Te led to a general increase in the absolute current values (~pA for sulfides compare to ~μA in tellurides), but simultaneously caused a decrease in the photosensitivity (from several orders of changes in the current magnitude under illumination for sulfides to ~1 order changes in tellurides).[39-45] The compositional dependence of photocurrents generated in Ge_xSe_{100-x} thin films by white light from a tungsten lamp shows a sharp maximum at the $Ge_{20}Se_{80}$ composition.[46] The same Ge content was deemed to be optimal in a Ge_xS_{100-x} system, where $Ge_{20}S_{80}$ thin films were used to investigate the Bi doping

effect on the photocurrent generated by a tungsten lamp illumination.[47] The $Ge_{20}(S/Se)_{80}$ composition is also known as the rigidity percolation point in respective binary glass-forming systems.[48,49] To improve glass-forming ability and enhance the effects associated with spin-orbit interactions (important in photovoltaics), Sb has been introduced into the composition. The conductivity of some ternary Sb-containing chalcogenides (Ge-Sb-S, $Ge_2Sb_2Te_5$)[45,50] is already shown to be quite sensitive to the light exposure, exhibiting a power-law illumination power dependence.[50]

Based on these experimental data, in our investigation we kept Ge content at the level of 20 at.% and experimented with various Sb/S/Se/Te ratios to optimize photosensitivity, optical transparency, and photocurrent response. This approach allowed us to develop Ge- and Sb-based amorphous film containing all three chalcogens in equal proportion (named equichalcogenides) that, in our opinion, has a huge potential in all-photonic platform, photovoltaic and sensor applications. The Ge-Sb-based thin films containing simultaneously 2 sorts of chalcogens in a composition are already shown to have tremendous prospects of applications in near and mid-infrared photonics and optical sensors, since their linear and nonlinear optical properties can be significantly tailored by composition.[30] Nevertheless, to the best of our knowledge, the equichalcogenides simultaneously containing all 3 sorts of chalcogen have not yet been studied.

2. EXPERIMENTAL SECTION

Bulk $Ge_{20}Sb_{20}S_{20}Se_{20}Te_{20}$ materials were prepared by the conventional melt quenching method using 5N-purity elements (Alfa Aesar, Umicore). The appropriate amounts of chemical precursors were vacuum sealed in 7 mm diameter silica ampoules, heated up to 850°C, homogenized at this temperature for 12 hours in a rocking furnace, and quenched into room temperature water. The obtained rods were crushed and loaded into tungsten boats of MBRAUN thermal evaporator to

vacuum deposit thin films. Microscopy glass slides, quartz wafers, and Si/SiO_2 chips with interdigitated gold electrodes (p-type monocrystalline silicon with 300 nm thick SiO_2 layer; 30 μm wide, and 10 nm/100 nm thick Cr/Au finger electrodes; 30 μm line spacing; 20 interdigitated pairs of 40 fingers) were used as substrates that were simultaneously mounted on a rotational holder of the evaporator. Thickness of the films and deposition rate were monitored in situ using the quartz crystal microbalance method implemented into MBRAUN evaporator system.

Compositions of the prepared films were checked using a scanning electron microscope (Hitachi S-4800 FESEM) equipped with an energy-dispersive spectroscopy (EDS) analyzer FEI QUANTA 3D 200i.

XPS spectra were recorded in normal emission mode using a high-resolution ESCALAB Xi+ spectrometer (Thermo Electron North America LLC) equipped with a monochromatic Al K_α (1486.6 eV) X-ray source under a vacuum of 10^{-8} Torr or better. The analysis area was ~500 μm spot and data acquisition was restricted electronically to a region smaller than the X-ray illuminated area. The energy scale of the instrument was calibrated using Fermi level of clean Ag. The surface charging from photoelectron emission was neutralized using a low energy (<10 eV) electron flood gun. The experimental positions of the valence band spectra were adjusted by referencing to the position of 1s core level peak (284.6 eV) of adventitious carbon and Ge Auger lines. X-ray diffraction (XRD) spectra were measured with the Rigaku Miniflex 6G system, equipped with an accessory for thin film XRD measurements at different temperatures.

Photoconductivity measurements were performed using the investigated film in series with Keithley 485 pico-ammeter and Agilent E3631A power supply. A correction on the dark photocurrent was applied before each measurement. The relative change in the current was calculated using the following: $I = \frac{I_{ph} - I_{dark}}{I_{dark}} * 100\%$.

A temperature-controlled vacuum chamber, Linkam (L-THMS350/EV-4), was used to mount the films during light exposure. This specially designed chamber allowed simultaneous electric current and optical spectroscopy measurements at low vacuum and different temperatures. The samples were exposed through the chamber's quartz window to various wavelengths of light ranging from 400 to 1000 nm and at various temperatures ranging from -50 to 125°C. Light for the exposure was obtained using a xenon short arc lamp of Horiba Fluorolog-3 spectrofluorimeter equipped with a grating monochromator. An appropriate set of filters has been used to cut higher orders diffraction maxima from the exposure spectrum, verified using the VIS spectrometer (Ocean Optics). The power of the incident light was controlled by a slit width of the spectrofluorimeter and measured with a power meter (Thorlabs PM100 with S130A sensor) placed directly at the location of the sample. It was either constant or chosen to keep a constant number of photons per second (flux) for each wavelength of the incident light.

Optical transmission spectra for absorption coefficient and bandgap calculations were measured by UV/VIS/NIR spectrophotometer Agilent Cary 5000 and Avantes (AvaSpec-ULS2048XL-2) fiber optic spectrometer in the case of temperature dependence.

3. RESULTS AND DISCUSSION

3.1. Basic Physical Properties

SEM image and EDS analysis of the prepared thin films (Figure 1 shows the film deposited on Si/SiO_2 substrate with interdigitated gold electrodes as an example) indicate that film composition is uniform (standard deviation of the composition across the film does not exceed 1 at.%) and very close (deviations do not exceed ±3 at.%) to the nominal composition of the target bulk material ($Ge_{20}Sb_{20}S_{20}Se_{20}Te_{20}$). The thickness of the deposited thin film, determined from the SEM image (Figure 1), is also close to the desired thickness of 1 μm. The XRD patterns show no significant

crystalline reflexes for both the as-prepared thin film and the film held at 175 ºC (Figure 2), allowing us to exclude from further consideration the irreversible crystallization processes during temperature-dependent photocurrent measurements (maximum temperature did not exceed 125 ºC). The beginning of crystallites formation/growth becomes noticeable in XRD spectra at the temperatures higher than 200 ºC, which can be inferred from XRD pattern recorded at 225 ºC (Figure 2, circled region). It can be emphasized that observed temperature stability interval of equichalcogenide films is larger than in $MAPbI_3$ or $MASnI_3$ perovskite materials, for example, having a number of possible phase transitions at temperatures higher than ~70 ºC.[51]

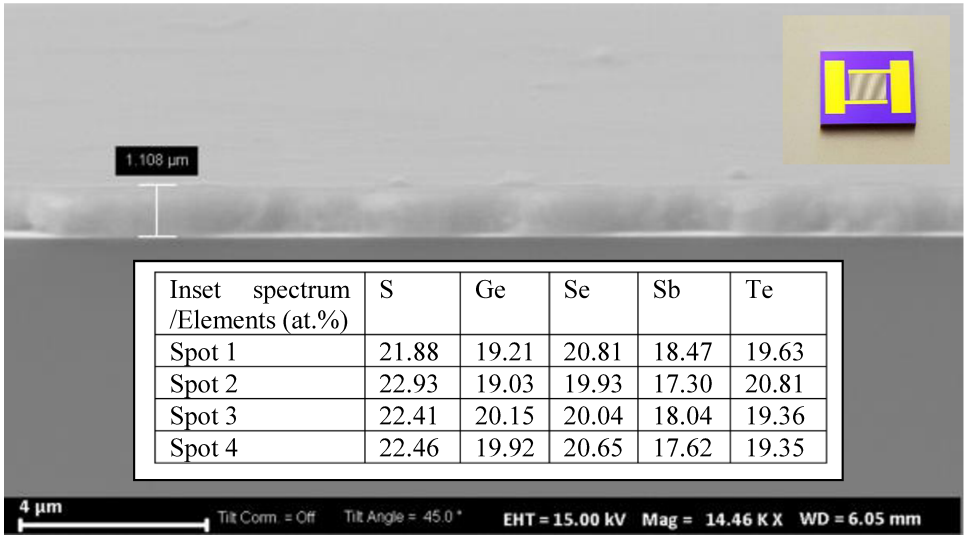

Inset spectrum /Elements (at.%)	S	Ge	Se	Sb	Te
Spot 1	21.88	19.21	20.81	18.47	19.63
Spot 2	22.93	19.03	19.93	17.30	20.81
Spot 3	22.41	20.15	20.04	18.04	19.36
Spot 4	22.46	19.92	20.65	17.62	19.35

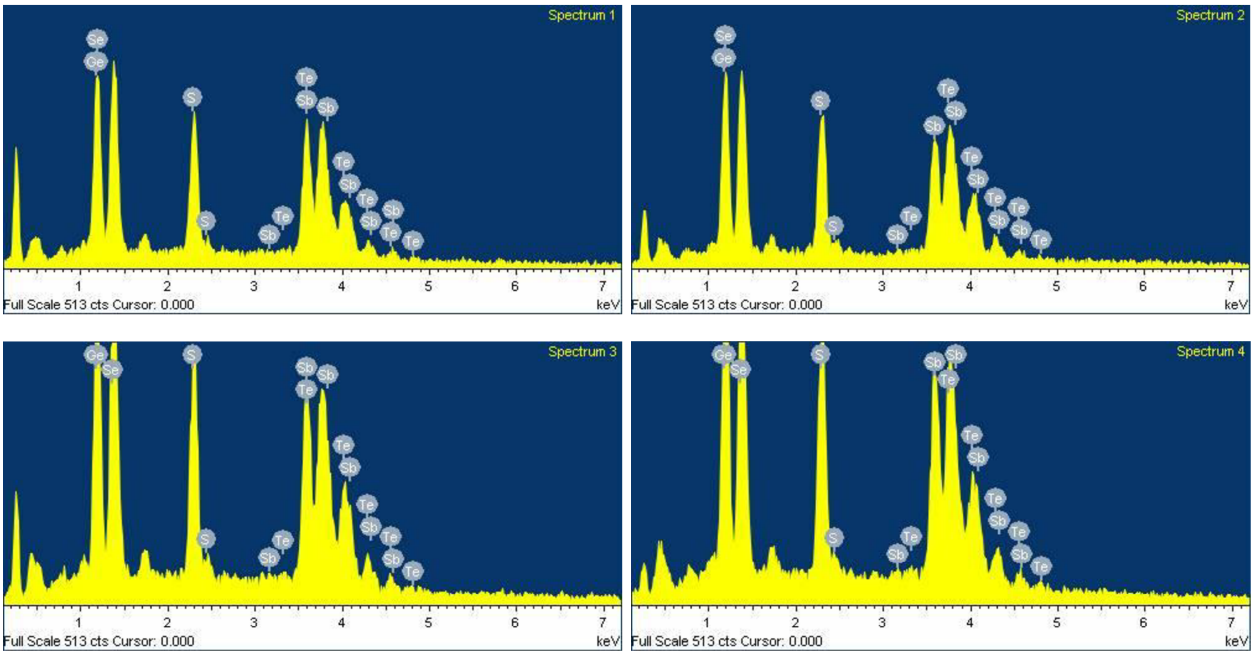

Figure 1. SEM image of the cross-section (fresh fracture) of thin film deposited on Si/SiO_2 substrate with interdigitated gold electrodes (optical image of substrate is shown at the right top). EDS spectra and compositional analysis (in at.%) are presented for 4 different spots (Spectra 1-4) on the film surface (peaks of Si and C are not included into analysis).

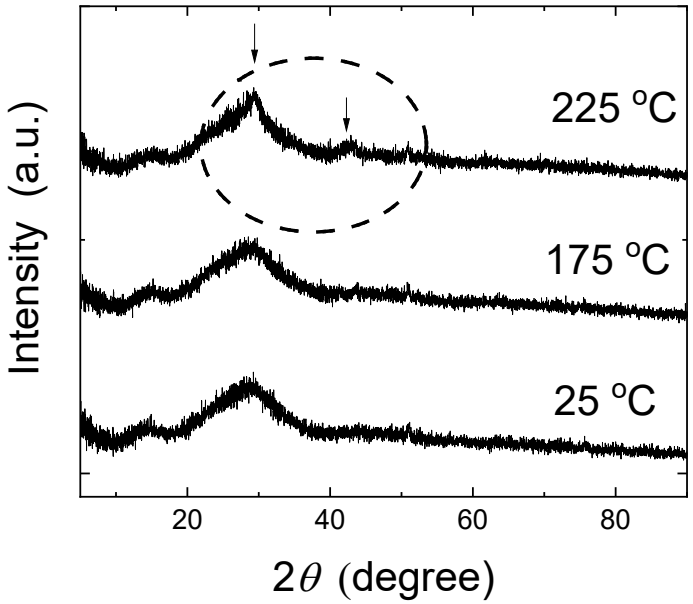

Figure 2. XRD patterns recorded at 25 °C, 175 °C and 225 °C temperatures for $Ge_{20}Sb_{20}S_{20}Se_{20}Te_{20}$ thin film deposited on microscopy slide substrate. The circled region shows the beginning of crystallites formation/growth at higher temperatures.

A typical room temperature optical transmission spectrum of the film deposited on a microscopy slide is shown in Figure 3a. Such a spectrum can be used to calculate the absorption coefficient (insert to Figure 3a) and Tauc plots. The optical bandgap values (E_g) at room temperature, as estimated from Tauc plots using PARAV,[52] are E_g = 1.705±0.005 eV and E_g = 1.330±0.005 eV for direct and indirect allowed transitions, respectively. These values are well comparable with the optical gaps of Sn- and Pb-based halide perovskites (usually found within 1.2-1.8 eV range),[51,53,54] considered to be excellent photovoltaic materials. Taking into account the color of the film and further photocurrent measurements, the 1.71±0.01 eV value can be accepted as the realistic optical gap, meaning that engineered material is, the most probably, direct bandgap semiconductor (although most of chalcogenide glasses are deemed as indirect bandgap semiconductors).[55]

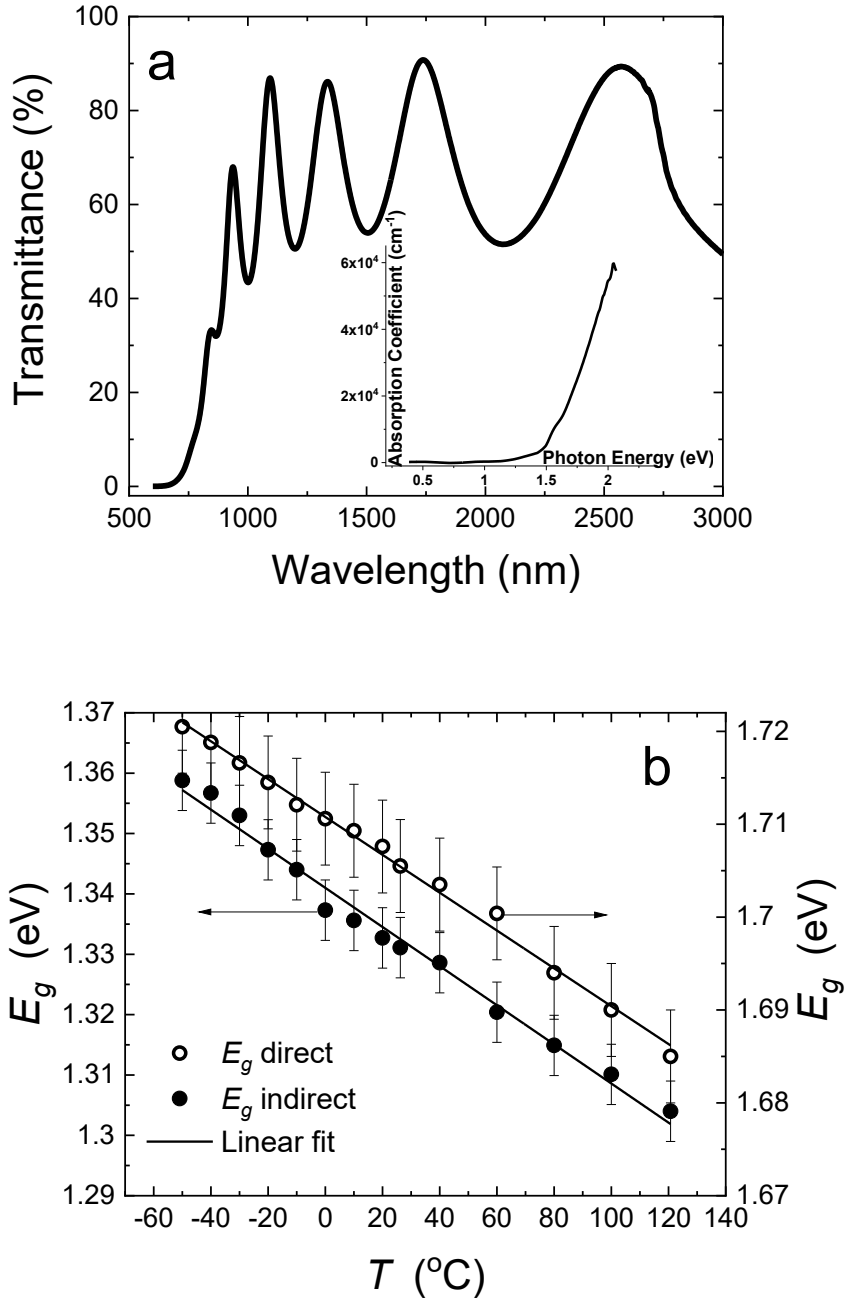

Figure 3. $Ge_{20}Sb_{20}S_{20}Se_{20}Te_{20}$ thin film deposited on microscopy slide substrate: (a) optical transmission spectrum recorded at room temperature and calculated absorption coefficient (insert); (b) temperature dependence of optical gap E_g estimated from Tauc plots for direct and indirect transitions.

The temperature dependence of the optical gap (Figure 3b), as estimated from the temperature dependence of optical transmission in the fundamental optical absorption edge region using

PARAV could be well fitted by a line with a slope of $(-3\pm1)\cdot10^{-4}$ eV/K. Linear dependence is typical for chalcogenide glasses and amorphous thin films in the considered temperature range.[56] The optical gap variation does not exceed 0.1 eV within the applied temperatures (Figure 3b), ensuring a good temperature stability of the $Ge_{20}Sb_{20}S_{20}Se_{20}Te_{20}$ film spectral sensitivity.

The temperature dependence of resistivity (ρ) for the as-deposited thin films is shown in Figure 4a for maximum and minimum bias voltages used for the photocurrent measurements. The dependence obeys the exponential law as expected for non-crystalline semiconductor materials at below-glass transition temperature (in the case of charge carriers excitation directly into the non-localized states of conduction band):[55]

$$\rho = \rho_0 e^{\frac{E_a}{k_B T}} \quad (1)$$

where k_B is Boltzmann constant, ρ_0 is a constant related to the effective density of states and the mobility gap, and E_a is the activation energy of conductivity that, in the case of relatively high temperatures, is approximately equal to the difference between the conduction band (E_c) and Fermi (E_F) energy levels.[55]

This activation energy was estimated at the average value of $E_a = 0.58\pm0.01$ eV for the investigated films, using a slope of linear part in $\ln(\rho)$ *vs* $1000/T$ plots (Figure 4a). Comparing this value to the obtained E_g from optical spectra, it can be concluded that Fermi level would be closer to the conduction band if the band-like charge carrier transport mechanism is mainly considered. The obtained activation energy of conductivity is very close to E_a = 0.65-0.7 eV of the $MAPbI_3$ perovskite film.[54] The resistivity values of the engineered $Ge_{20}Sb_{20}S_{20}Se_{20}Te_{20}$ thin films (~10^7-10^9 Ω·cm, Figure 4a) are also comparable to those of halide perovskite materials.[51,54]

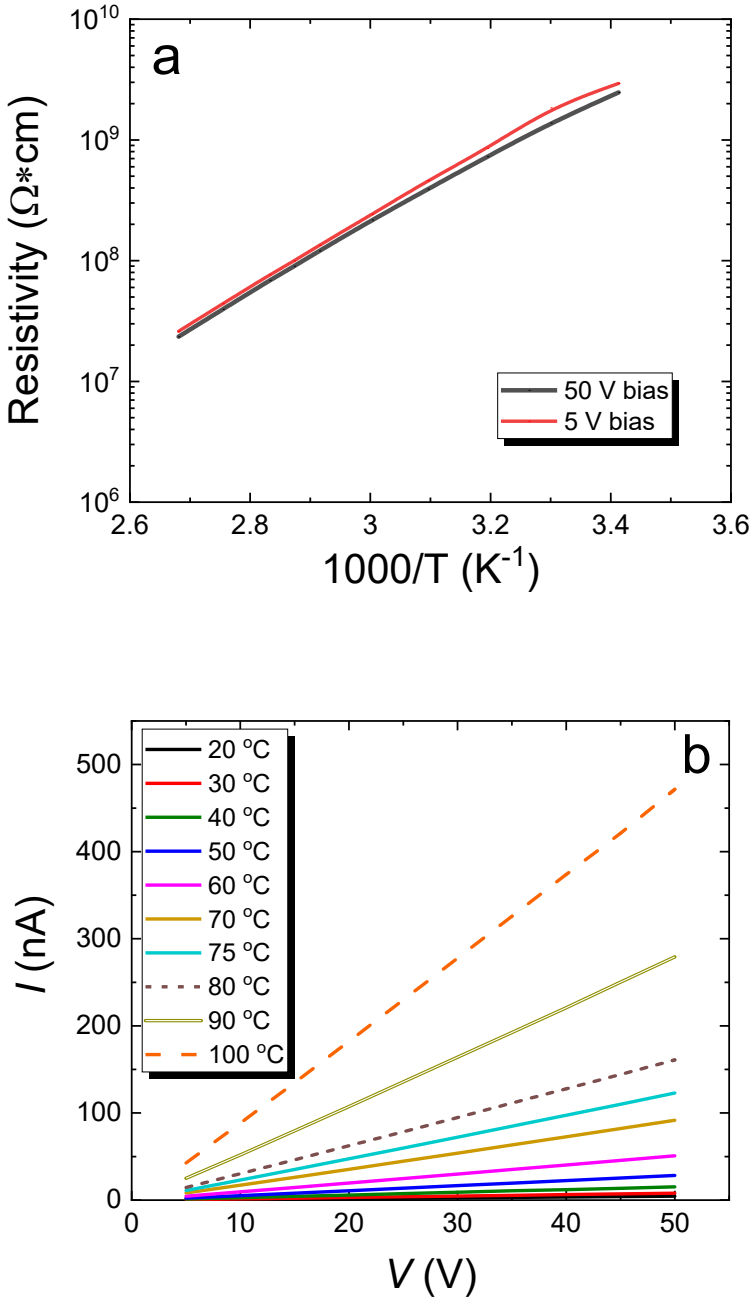

Figure 4. Temperature dependence of dark resistivity (a) and Ohmic part of dark V-I characteristics recorded at different temperatures (b) for $Ge_{20}Sb_{20}S_{20}Se_{20}Te_{20}$ thin film on Si/SiO_2 substrate with interdigitated gold electrodes.

The volt-ampere (V-I) characteristics of the prepared device are shown in Figure 4b for different temperatures. They are linear (Ohmic) in the applied 5-50 V bias voltage range.

3.2. Photocurrent and Possible Mechanisms

The exposure to light with different wavelengths alters V-I characteristics as shown in Figure 5a, but the linearity within the considered voltage bias range remains. The exposure at the elevated temperatures increases the overall current in the film (Figure 5b), but simultaneously decreases light sensitivity (relative changes caused by photoexposure are smaller). The photocurrent values are within a tenth to a hundredth of the μA range, making them high enough to be confidently measured but also low enough to ensure a low power consumption of the sensor.

Huge relative changes in the electrical current were observed within the entire range of the exposure wavelengths (Figure 6), indicating perfect sensitivity of the engineered material to the incident light from all visible and NIR spectra. The magnitude of the observed changes is remarkably flat across the above-bandgap (400-700 nm) range of exposure wavelengths and declines for the wavelengths of light with energies smaller than the estimated direct band gap of the material (Figure 6a). This decline, however, is not as abrupt as in the case of binary and doped chalcogenides studied so far.[39-45] It is also not so steep as in the case of $MAPbI_3$ perovskites,[54] so it could potentially allow the harvest of more light from below bandgap wavelengths if $Ge_{20}Sb_{20}S_{20}Se_{20}Te_{20}$ thin films were used as photovoltaics.

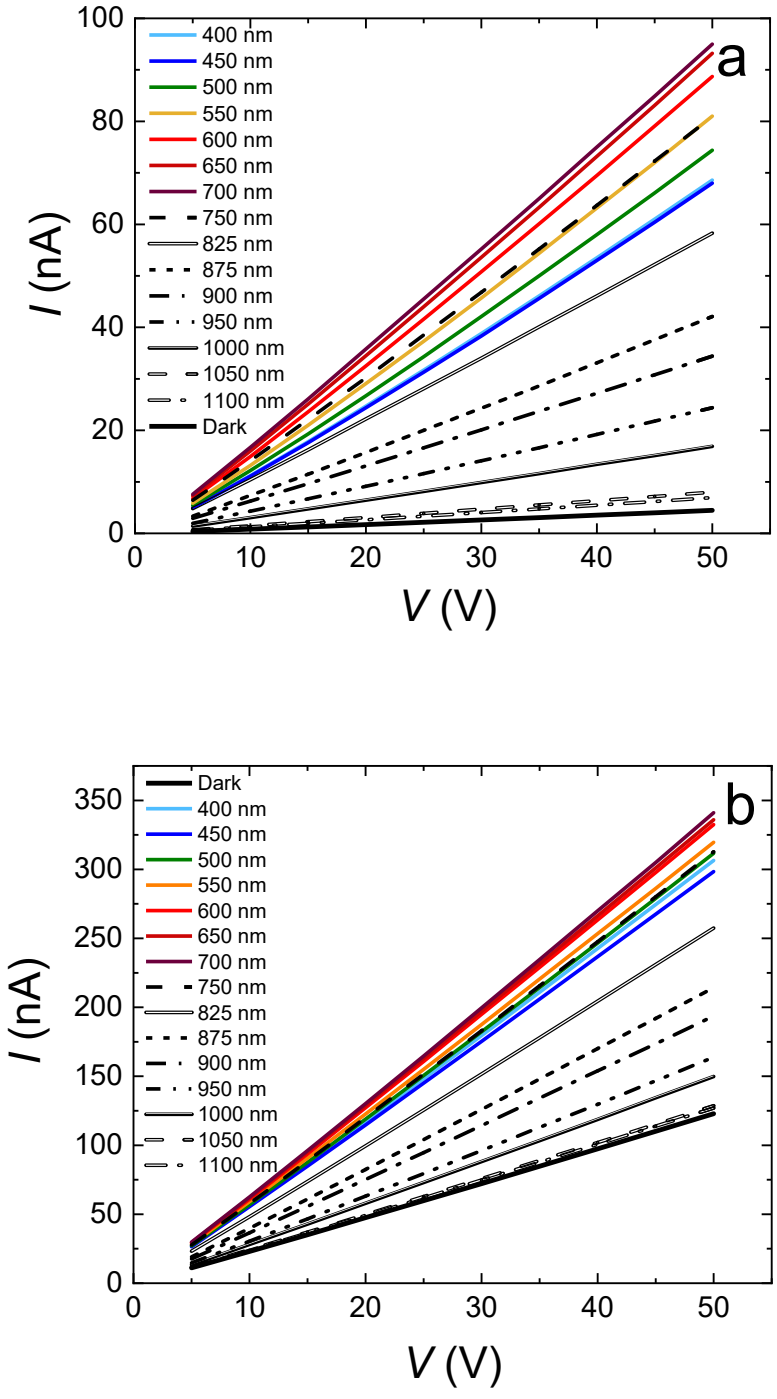

Figure 5. Ohmic parts of V-I characteristics for $Ge_{20}Sb_{20}S_{20}Se_{20}Te_{20}$ thin film on Si/SiO_2 substrate with interdigitated gold electrodes recorded at 20 °C (a) and 75 °C (b) under 3.795 mW/cm^2 constant power exposure with light of different wavelengths.

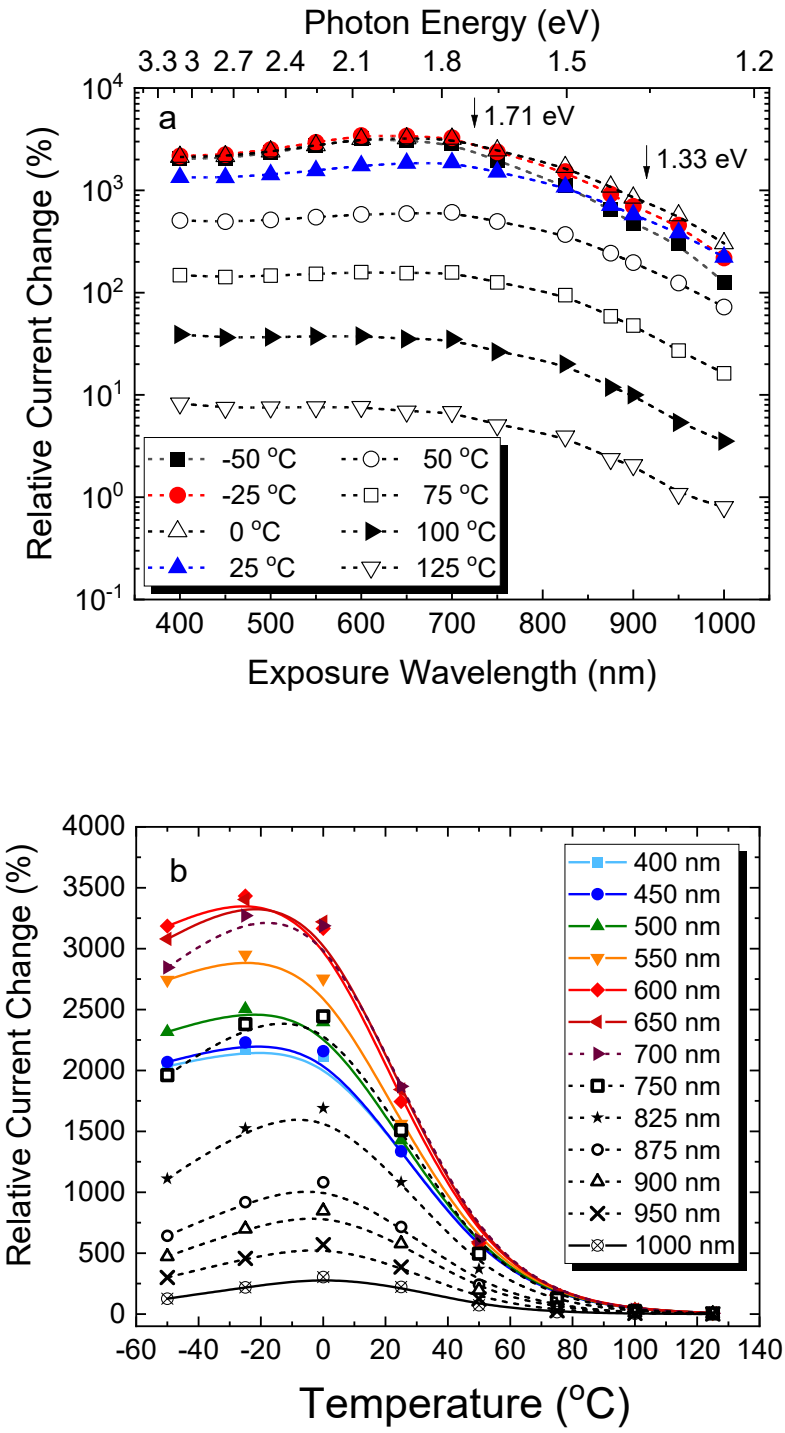

Figure 6. Relative current change as a function of wavelength (a) and temperature (b) measured for $Ge_{20}Sb_{20}S_{20}Se_{20}Te_{20}$ thin film deposited on Si/SiO_2 substrate with interdigitated gold electrodes, using 20 V bias voltage and constant flux ($1.704 \cdot 10^{16}$ photons$\cdot s^{-1} \cdot cm^{-2}$) for the exposure with each wavelength. Curves are drawn as a guide to the eyes.

To understand this behavior, it is worth considering the possible processes occurring in chalcogenide materials under photoexposure. The first step of interaction of the radiation (UV, VIS, NIR light, neutrons, γ- or X-rays) with the chalcogenide substance is almost always energy absorption, excitation of electrons and/or holes, displacement of atoms, and creation or amplification of phonons. Such processes can lead to chemical bond redistribution or reorientation, photo-induced crystallization or amorphization, formation of products of synthetic or photolytic chemical reactions, electronic or atomic defects, changes in chemical reactivity, surface profile, optical transmittivity and reflectivity, index of refraction, hardness, thickness, fluidity, etc.[3,5,9,33,34,37,38] In the case of above-bandgap exposure of the investigated material, the main mechanism is similar to crystalline semiconductors and is associated with light-induced generation of the charge carriers. When the energy of an incident photon exceeds the bandgap value, the electrons from top energy levels in the valence band are directly excited into the conduction band producing electron-hole pairs and broken covalent bonds. Owing to a low penetration depth of the above-bandgap light and the low mobility of electrons in chalcogenide glasses (usually these materials possess *p*-type of conductivity),[2,55] these excitations should be effective only in the surface layers of the sample where the above-bandgap incident light is directly absorbed. However, thermalization of the excited electrons through inelastic collisions with surrounding atoms, along with the switching/restoration of broken covalent bonds, would lead to the generation of phonons that can be absorbed by charge carriers in shallow energy traps (note, chalcogenides are characterized by a strong electron-phonon coupling)[2,55] abundant in amorphous chalcogenides. This process would lead to the enhancement of conductivity at above bandgap light exposure compared to the crystalline counterparts. We believe the number of shallow energy traps increases when more than one sort of chalcogen atoms is used in the composition. The indirect proof for

such a mechanism can be found in the physical aging studies of chalcogenide glasses, where above-bandgap light produces changes measurable by differential scanning calorimetry (bulk sensitive technique).[33,34] In the case of below bandgap light exposure, the energy of the incident photons is not enough to excite electrons from valence to conduction bands directly. The probability of bond breaking is also low. Therefore, only weak two-photon absorption processes, phonon-assisted electronic transitions, and inelastic photon scattering can cause the generation of charge carriers. However, prone to a much greater penetration depth of sub-bandgap light, these processes occur in a whole volume of the sample and not only in the surface layers as in the case of above-bandgap photoexposure. Therefore, sub-bandgap light can also produce a considerable amount of charge carriers because of greater statistics of the photo-perturbation events (more network sites are involved). Again, strong electron-phonon coupling and abundancy of charge carriers trapped in shallow energy levels compare to crystalline materials, allow the enhancement of conductivity in the below-bandgap light exposure regime.

To shed more light on why the equichalcogenides have different spectral characteristics of photoconductivity from binary and ternary chalcogenides or crystalline counterparts, their valence band structures, as obtained from the XPS, are compared in Figure 7. The lone pair (*lp*) electrons of chalcogen atoms (S, Se and Te) contribute to a density-of-state maximum at about 2 eV, showing an XPS peak that is broader than in the case of glasses containing only one sort of chalcogens. The same can be concluded for the density-of-state maximum at about 5 eV that occurs due to the broadening of S 3*p*, Se 4*p* and Te 5*p* bonding state peaks by chalcogen–metal (Ge,Sb) bonds.[35] Metal-metal bonds (like Ge-Ge, Ge-Sb or Sb-Sb) should have their dominant contribution at ~3.5 eV which can be ascertained from a comparison to the XPS valence band spectrum of $Ge_{22.2}Sb_{22.2}Te_{55.6}$ (GST-225)[57] phase change material (Figure 7). A remarkable feature of the

engineered $Ge_{20}Sb_{20}S_{20}Se_{20}Te_{20}$ thin film is its nearly uniform density of states distribution across the entire 0-6 eV energy interval, which might be a reason for extended photosensitivity of these films. Such overlap between the states is well consistent with recent theoretical analysis and predictions, made on the basis of halide perovskites studies, for the engineering of superior photovoltaic material.[58] The availability of deeper levels below the energy levels of lone pair electrons increases the chance of electron excitation into a conduction band without a significant residual kinetic energy when a high-energy photon is absorbed, making it possible to obtain a significant number of charge carriers in the conduction band without increasing the overall temperature of the semiconductor (usually occurs due to thermalization of "hot" electrons). It is important because an increase in temperature leads to a decrease in light sensitivity of the engineered film at all wavelengths (Figure 6b). In fact, the relative changes in a photocurrent become negligibly small if the temperature of the film during exposure to a low-power (~mW range) light exceeds ~120 ºC. This can be explained by a quite high dark current generated in the $Ge_{20}Sb_{20}S_{20}Se_{20}Te_{20}$ thin film due to a temperature-activated charge carriers' excitation directly into the non-localized states of the conduction band.

Although the obtained photoresponse of the fabricated device is within ~mA/W range, which is lower than photoresponse of Silicon- or Graphene-based devices,[59] it is high enough for use in low-power consuming electronics and can be further improved in design (p-n, p-i-n junctions, Field-Effect Transistor configuration), as well as in the parameters optimization (substrate, number and shape of the electrodes, film thickness, effective area, patterning). The main advantages include having a uniform photoresponse over a broader wavelength range compared to Silicon and an amorphous nature of the medium that allows fine tailoring of physical and chemical properties through composition variation, doping with rare-Earth elements (similar

matrixes are proven to have their good solubility)[60] or formation of nanodots/nanoparticles/nanocavities/surface patterns.[6,15,61,62] Such modifications can significantly boost photoresponse or energy conversion in the desired wavelength range. The other remarkable feature that distinguishes this medium from Si-biased applications is its true multifunctionality. Thus, by changing Sb content alone, the proposed medium can be turned into a phase-change memory device, an IR optical waveguide, or a photoconductor. The developed material is transparent up to ~12 μm and has high index of refraction combined with high optical nonlinearity[30] making it a universal medium for integration in all-chalcogenide photonic devices.[15, 22-24]

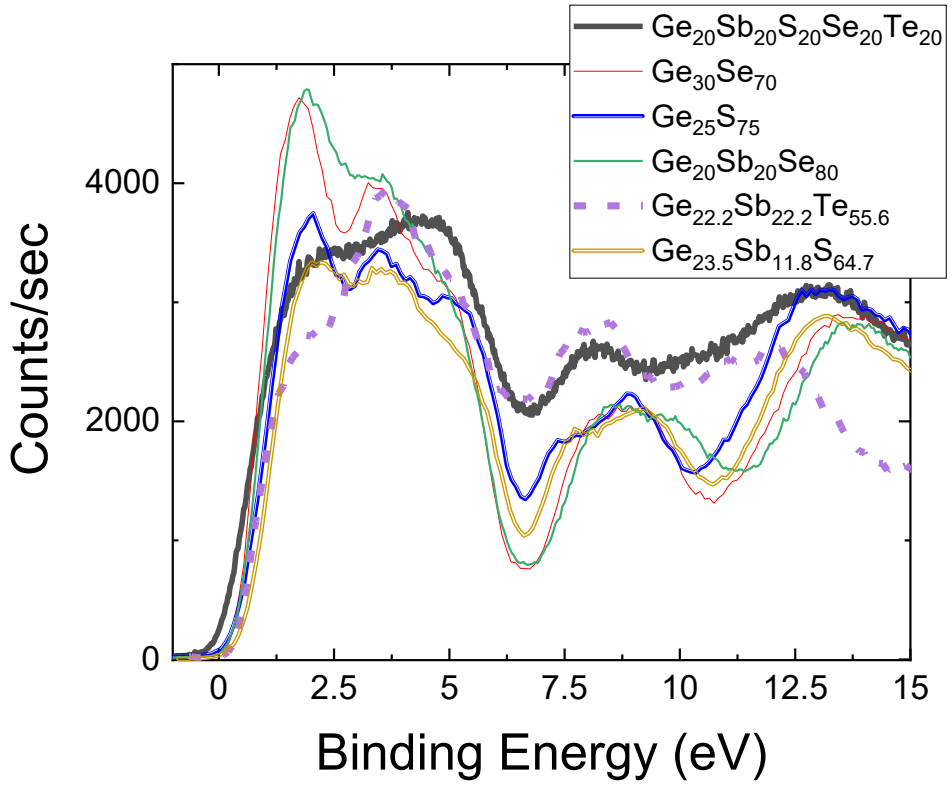

Figure 7. Valence band XPS spectra of the investigated film compared to the valence band XPS spectra of related chalcogenides.[35-37]

4. CONCLUSION

Multicomponent Ge- and Sb-based equichalcogenide (containing equal amount of S, Se and Te in the composition) thin films can be obtained using conventional thermal evaporation in the vacuum technique. Their optical properties are consistent with the requirements for all-chalcogenide photonic, sensor and photovoltaic materials. The $Ge_{20}Sb_{20}S_{20}Se_{20}Te_{20}$ films show superior light sensitivity in the 400-1000 nm wavelength range and in a broad temperature interval (up to 125 ºC). Relative changes in a photocurrent achieve thousands of percent at room and below-room temperatures under the exposure to light of only a few mW of power, making the material a very appealing medium for light sensors integrated into electronic and photonic circuits/arrays. Temperature dependence of resistivity in the -50 ºC – 120 ºC temperature diapason follows the exponential law for the broad range (5-50 V) of applied bias voltages. The volt-ampere (V-I) characteristics of $Ge_{20}Sb_{20}S_{20}Se_{20}Te_{20}$ thin films show linear (Ohmic) dependence within this bias voltage range. The exposure to light of different wavelengths change the slope of the V-I characteristics, but Ohmic character remains. Exposure at the elevated temperatures increases the overall current in the film, but simultaneously decreases light sensitivity, which vanishes above 120 ºC for the used exposure power. The engineered material is proposed as a perspective candidate for multifunctional integrated electronic/photonic devices, energy conversion and sensor applications.

AUTHOR INFORMATION

Corresponding Author

Roman Golovchak*
Department of Physics, Engineering and Astronomy, Austin Peay State University, Clarksville, TN 37044, USA
E-mail: holovchakr@apsu.edu

Author Contributions

The manuscript was written through contributions of all authors. All authors have given approval to the final version of the manuscript.

Funding Sources

The authors acknowledge support of National Science Foundation (NSF project OISE-2106457). TI and AT acknowledge the Joint School of Nanoscience and Nanoengineering, a member of the South-eastern Nanotechnology Infrastructure Corridor (SENIC) and the National Nanotechnology Coordinated Infrastructure (NNCI), supported by the NSF (grant ECCS-1542174).

Notes

The authors declare no competing financial interest.

ACKNOWLEDGMENTS

PJ thanks to the CUR Physics and Astronomy (CURPA) Division, through the Nadine Barlow Undergraduate Research Support Award.

REFERENCES

(1) *Amorphous semiconductor technologies and devices*; Hamakawa, Y., Ed.; OHM Ltd. and North Holland Publishing Co., **1988**.
(2) Feltz, A. *Amorphous Inorganic Materials and Glasses*; VCH, Weinheim, **1993**.
(3) Kolobov, A.V. *Photoinduced metastability in amorphous semiconductors;* WILEY-VCH GmbH & Co.KGaA, Weinheim, **2003**.

(4) Borisova, Z. U. *Glassy semiconductors*; Plenum Press, New York and London, **1981**.

(5) Popescu, M. *Non-crystalline chalcogenides*; Kluwer Academic Publishers, New York, **2002**.

(6) *Chalcogenide Glasses: Preparation, properties and application*; Adam, J-L.; Zhang X., Eds.; Woodhead Publishing series in Electronic and Optical Materials No.44, **2014**.

(7) *Amorphous chalcogenides: advances and applications*; Wang, R.P., Ed.; Pan Stanford Publishing Pte. Ltd., Singapore, **2014**.

(8) Lyubin, V.; Klebanov, M.; Feigel, A.; Sfez, B. Films of chalcogenide glassy semiconductors: New phenomena and new applications. *Thin Solid Films* **2004**, *459*, 183–186.

(9) Lencer, D.; Salinga, M.; Wuttig, M. Design rules for phase-change materials in data storage applications. *Adv. Mater*. **2011**, *23*, 2030–2058.

(10) Wuttig, M.; Yamada, N. Phase-change materials for rewritable data storage. *Nat. Mater.* **2007**, *6*, 824–832.

(11) Zhang, X.; Bureau, B.; Lucas, P.; Boussard-Pledel, C.; Lucas, J. Glasses for seeing beyond visible. *Chem. Eur. J.* **2008**, *14* 432–442.

(12) Bureau, B.; Zhang, X.H.; Smektala, F.; Adam, J.-L.; Troles, J.; Ma, H.; Boussard-Pledel, C.; Lucas, J.; Lucas, P.; Coq, D.L.; Riley, M.R.; Simmons, J.H. Recent advances in chalcogenide glasses. *J. Non-Cryst. Solids* **2004**, *345&346*, 276.

(13) Xu, P.; Zheng, J.; Doylend, J.K.; Majumdar, A. Low-loss and broadband nonvolatile phase-change directional coupler switches. *ACS Photonics* **2019**, *6*, 553–557.

(14) Wang, Q.; Rogers, E.T.F.; Gholipour, B.; Wang, Ch.-M.; Yuan, G.; Teng, J.; Zheludev, N.I. Optically reconfigurable metasurfaces and photonic devices based on phase change materials. *Nat. Photonics* **2016**, *10*, 60–65.

(15) Hu, J.; Gu, T.; Shalaginov, M.; Yang F. (Massachusetts Institute of Technology, Cambridge, MA), Meta-Optics-Based Systems and Methods for Ocular Applications. US 2022/0110522 A1, **2022**.

(16) Dong, W.; Qiu, Y.; Zhou, X.; Banas, A.; Banas, K.; Breese, M.B.H.; Cao, T.; Simpson, R.E. Tunable mid-infrared phase-change metasurface. *Adv. Optical Mater.* **2018**, *6*, 1701346.

(17) Gholipour, B.; Zhang, J.; MacDonald, K. F.; Hewak, D.W.; Zheludev, N.I. An all-optical, non-volatile, bidirectional, phase-change meta-switch. *Adv. Mater.* **2013**, *25*, 3050–3054.

(18) Tittl, A.; Michel, A.-K.U.; Schäferling, M.; Yin, X.; Gholipour, B.; Cui, L.; Wuttig, M.; Taubner, T.; Neubrech, F.; Giessen, H. A switchable mid-infrared plasmonic perfect absorber with multispectral thermal imaging capability. *Adv. Mater.* **2015**, *27*, 4597–4603.

(19) Michel, A.-K. U.; Chigrin, D.N.; Maß, T.W.W.; Schönauer, K.; Salinga, M.; Wuttig, M.; Taubner, T. Using low-loss phase-change materials for mid-infrared antenna resonance tuning. *Nano Lett.* **2013**, *13*, 3470–3475.

(20) Zhang, Y.; Chou, J.B.; Li, J.; Li, H.; Du, Q.; Yadav, A.; Zhou, S.; Shalaginov, M.Y.; Fang, Zh.; Zhong, H.; Roberts, Ch.; Robinson, P.; Bohlin, B.; Ríos, C.; Lin, H.; Kang, M.; Gu, T.; Warner, J.; Liberman, V.; Richardson, K.; Hu, J. Broadband transparent optical phase change materials for high-performance nonvolatile photonics. *Nature Comm*. **2019**, *10*, 4279.

(21) Wuttig, M.; Bhaskaran, H.; Taubner, T. Phase-change materials for nonvolatile photonic applications. *Nat. Photonics* **2017**, *11*, 465–476.

(22) Eggleton, B. J.; Luther-Davies, B.; Richardson, K. Chalcogenide photonics. *Nat. Photonics* **2011**, *5*, 141–148.

(23) Ríos, C.; Stegmaier, M.; Hosseini, P.; Wang, D.; Scherer, T.; Wright, C.D.; Bhaskaran, H.; Pernice, W.H.P. Integrated all-photonic non-volatile multi-level memory. *Nat. Photonics* **2015**, *9*, 725–732.

(24) Wuttig, M.; Bhaskaran, H.; Taubner, T. Phase-change materials for nonvolatile photonic applications. *Nat. Photonics* **2017**, *11*, 465–476.

(25) Xu, B.; Qi, Sh.; He, P.; Ma, J. Antimony- and Bismuth-Based Chalcogenides for Sodium-Ion Batteries. *Chem. Asian J.* **2019**, *14*, 2925 – 2937.

(26) Zhang, Zh.; Shao, Yu.; Lotsch, B.; Hu, Y.-Sh.; Li, H.; Janek, J.; Nazar, L.F.; Nan, C.-W.; Maier, J.; Armand, M.; Chen, L. New horizons for inorganic solid state ion conductors. *Energy Environ. Sci.* **2018**, *11*, 1945.

(27) Cui, S.; Boussard-Plédel, C.; Troles, J.; Bureau, B. Telluride glass single mode fiber for mid and far infrared filtering. *Opt. Mater. Express* **2016**, *6*, 971.

(28) Cui, Sh.; Chahala, R.; Shpotyuk, Ya.; Boussard, C.; Lucas, J.; Charpentier, F.; Tariel, H.; Loréal, O.; Nazabal, V.; Sire, O.; Monbet, V.; Yang, Zh.; Lucas, P.; Bureau, B. Selenide and telluride glasses for mid-infrared bio-sensing. *Proc. of SPIE* **2014**, *8938*, 893805.

(29) Petersen, C.R.; Moller, U.; Kubat, I.; Zhou, B.; Dupont, S.; Ramsay, J.; Benson, T.; Sujecki, S.; Abdel-Moneim, N.; Tang, Z.; Furniss, D.; Seddon, A.; Bang, O. Mid-infrared supercontinuum covering the 1.4–13.3 μm molecular fingerprint region using ultra-high NA chalcogenide step-index fibre. *Nat. Photon.* **2014**, *8*, 830–834.

(30) Dory, J.-B.; Castro-Chavarria, C.; Verdy, A.; Jager, J.-B.; Bernard, M.; Sabbione, C.; Tessaire, M.; Fédéli, J.-M.; Coillet, A.; Cluzel, B.; Noé, P. Ge–Sb–S–Se–Te amorphous chalcogenide thin films towards onchip nonlinear photonic devices. *Sci. Reports* **2020**, *10*, 11894.

(31) Saturday, L.; Johnson, C.; Thai, A.; Szlęzak, J.; Shpotyuk, Y.; Golovchak, R. Devitrification of Bi- and Ga-containing germanium-based chalcogenide glasses. *J. Alloys Compd.* **2016**, *674*, 207–217.

(32) Golovchak, R.; Kozdras, A.; Hodge, T.; Szlęzak, J.; Boussard-Pledel, C.; Shpotyuk, Ya.; Bureau, B. Optical and thermal properties of Sb/Bi-modified mixed Ge-Ga-Se-Te glasses. *J. Alloys and Compd*. **2018**, *750*, 721-728.

(33) Kozdras, A.; Golovchak, R.; Shpotyuk, O.; Szymura, S.; Saiter, A.; Saiter, J.-M. Light-assisted physical ageing in chalcogenide glasses: dependence on the wavelength of incident photons. *J. Mater. Res.* **2011**, *26*, 2420-2427.

(34) Golovchak, R.; Kozdras, A.; Shpotyuk, O. Physical ageing in glassy As-Se induced by above-bandgap photoexposure. *Solid State Commun.* **2008**, *145*, 423-426.

(35) Kozyukhin, S.; Golovchak, R.; Kovalskiy, A.; Shpotyuk, O.; Jain, H. Valence band structure of binary chalcogenide vitreous semiconductors by high-resolution XPS. *Semiconductors* **2011**, *45*, 423-426.

(36) Sati, D.; Kovalskiy, A.; Golovchak, R.; Jain, H. Structure of $Sb_xGe_{40-x}Se_{60}$ glasses around 2.67 average coordination number. *J. Non-Cryst. Solids* **2012**, *358*, 163-167.

(37) Kovalskiy, A.P.; Jain, H.; Miller, A.C.; Golovchak, R.Ya.; Shpotyuk, O.I. A study of reversible γ-induced structural transformations in vitreous $Ge_{23.5}Sb_{11.8}S_{64.7}$ by high-resolution X-ray photoelectron spectroscopy. *J. Phys. Chem. B* **2006**, *110*, 22930-22934.

(38) Golovchak, R.; Shpotyuk, O. Radiation-induced bond switching in mixed Ge-As sulphide glasses. *Phil. Magazine* **2005**, *85*, 2847-2860.

(39) Toyosawa, N.; Tanaka, K. Photocurrent enhancement in light-soaked chalcogenide glasses. *Phys. Rev. B* **1997**, *56*, 7416.

(40) Toyosawa, N.; Tanaka, K. Photocurrent enhancement in light-soaked As_2S_3 glass. *Solid State Commun.* **1996**, *97*, 623-626.

(41) Stuke, J. Review of optical and electrical properties of amorphous semiconductors. *J. Non-Cryst. Solids* **1970**, *4*, 1-26.

(42) Sawan, Y.; Wakim, F.; El-Gabaly, M.; Prasad, R. Electrical and photoconductive properties of the $As_2Se_3Bi_x$ System. *J. Non-Cryst. Solids* **1979**, *30*, 293-300.

(43) Bletskan, D.I.; Kabatsiy, V.N.; Frolova, V.V. Peculiarities of the absorption edge and Photoconductivity spectra of $(GeS_2)_x(Bi_2S_3)_{1-x}$ glasses. *Chalcogenide Letters* **2007**, *4*, 119 – 126.

(44) Scharnhorst, K.P.; Riedl, H. R. Photoconductivity in the amorphous Ge-rich Ge_xTe_{1-x} system. *J. Appl. Phys.* **1974**, *45*, 2971.

(45) Rütten, M.W. *Underlying mechanisms of resistance drift in amorphous phase-change materials,* Aachen University (Germany), **2020**.

(46) Kumar, A.; Goel, S.; Tripathi, S. K. Steady-state and transient photoconductivity in amorphous thin films of Ge_xSe_{100-x}. *Phys. Rev B* **1988**, *38*, 13432.

(47) Abd El-Salam, F.; Fadel, M.; Sedeek, K. Temperature and thickness dependence of photoconductivity and density-of-states distribution for Bi doped $Ge_{20}S_{80}$. *Vacuum* **1994**, *45*, 835-839.

(48) Golovchak, R.; Shpotyuk, O.; Kozyukhin, S.; Kovalskiy, A.; Miller, A.C.; Jain, H. Structural paradigm of Se-rich Ge-Se glasses by high-resolution X-ray photoelectron spectroscopy. *J. Appl. Phys.* **2009**, *105*, 103704 (7).

(49) Shpotyuk, O.; Golovchak, R. Pseudo-self-organized topological phases in glassy selenides for IR photonics. *Phys. Stat. Solidi C* **2011**, *8*, 2572-2576.

(50) Kumeda, M.; Kawachi, G.; Shimizu, T. Photoconductivity and photoluminescence and their relation to light-induced ESR in $(Ge_{0\cdot42}S_{0\cdot58})_{1-x}(Sb_{0\cdot4}S_{0\cdot6})_x$ glasses. *Phil. Mag. B* **1985**, *51*, 591-602.

(51) Stoumpos, C.C.; Malliakas, Ch.D.; Kanatzidis, M.G. Semiconducting Tin and Lead Iodide Perovskites with Organic Cations: Phase Transitions, High Mobilities, and Near-Infrared Photoluminescent Properties. *Inorg. Chem.* **2013**, *52*, 9019−9038.

(52) Ganjoo, A.; Golovchak, R. Computer program PARAV for calculating optical constants of thin films and bulk materials: Case study of amorphous semiconductors. *J. Optoelectronics Adv. Materials* **2008**, *10*, 1328-1332.

(53) De Wolf, S.; Holovsky, J.; Moon, S.-J.; Löper, Ph.; Niesen, B.; Ledinsky, M.; Haug, F.-J.; Yum, J.-H.; Ballif, Ch. Organometallic Halide Perovskites: Sharp Optical Absorption Edge and Its Relation to Photovoltaic Performance. *J. Phys. Chem. Lett.* **2014**, *5*, 1035−1039.

(54) Khenkin, M. V.; Amasev, D. V.; Kozyukhin, S. A.; Sadovnikov, A. V.; Katz, E. A.; Kazanskii, A. G. Temperature and spectral dependence of $CH_3NH_3PbI_3$ films photoconductivity. *Appl. Phys. Lett.* **2017**, *110*, 222107.

(55) *Electronic processes in non-crystalline materials,* (Eds: Mott, N.; Davis, E.), Oxford University press, New York, **1979**.

(56) Forsythe, J.; Shpotyuk, M.; Shpotyuk, O.; Golovchak, R. On the temperature behavior of optical gap in arsenic sulphide glasses. *Phys. Status Solidi B* **2022**, *259*, 2100404.

(57) Golovchak, R.; Choi, Y.G.; Kozyukhin, S.; Chigirinsky, Yu.; Kovalskiy, A.; Xiong-Skiba, P.; Trimble, J.; Pafchek, R.; Jain, H. Oxygen incorporation into GST phase-change memory matrix. *Appl. Surf. Sci.* **2015**, *332*, 533–541.

(58) Wuttig, M.; Schön, C.-F.; Schumacher, M.; Robertson, J.; Golub, P.; Bousquet, E.; Gatti, C.; Raty, J.-Y. Halide Perovskites: Advanced Photovoltaic Materials Empowered by a Unique Bonding Mechanism. *Adv. Funct. Mater.* **2022**, *32*, 2110166.

(59) Wu, C.; Wu, F.; Hu, H.; Ma, C.; Ye, J.; Wang, S.; Wu, H.; Wang, J.; Liu, A.; Guo, D. Work function tunable laser induced graphene electrodes for Schottky type solar-blind photodetectors. *Appl. Phys. Lett.* **2022,** *120*, 101102.

(60) Je Park, B.; Seo, H.S.; Ahn, J.T.; Choi, Y.-G.; Jeon, D.Y.; Chung, W.J. Mid-infrared (3.5–5.5 μm) spectroscopic properties of Pr^{3+}-doped Ge–Ga–Sb–Se glasses and optical fibers. *J. Luminescence* **2008**, *128*, 1617-1622.

(61) Khan, Z.H.; Al-Ghamdi, A.A.; Al-Agel, F.A. Crystallization kinetics in as-synthesis high yield of a-Se100−xTex nanorods. *Mat. Chem. Phys.* **2012**, *134*, 260-265.

(62) Golovchak, R.; Shpotyuk, Ya.; Szlęzak, J.; Dziedzic, A.; Ingram, A.; Cebulski, J. Giant visible and infrared light attenuation effect in nanostructured narrow-bandgap glasses. *Optics Letters* **2018**, *43*, 387-390.

For Table of Contents only

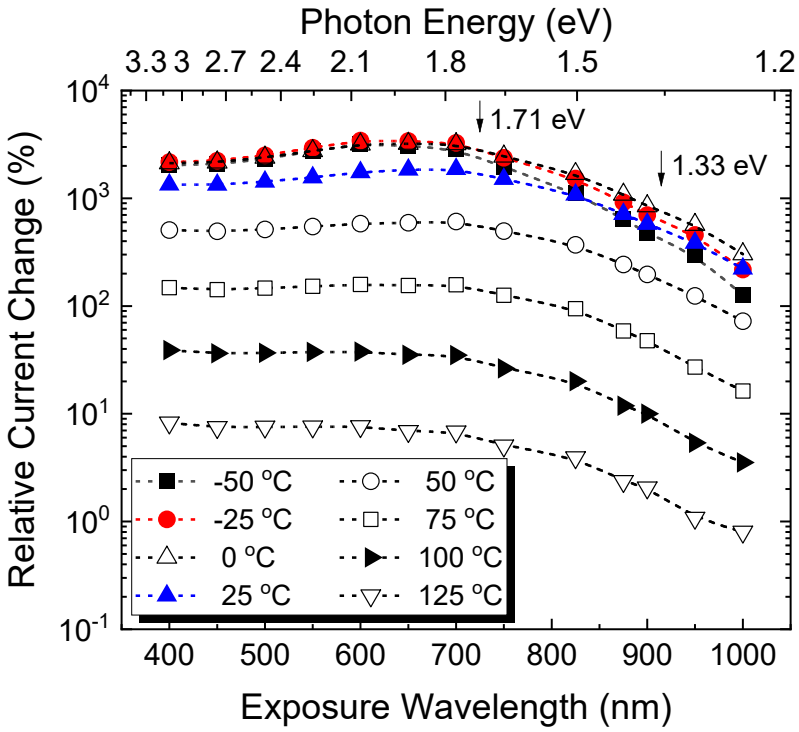

Relative current change as a function of exposure wavelength, measured at different temperatures.